Retina

Comparison Between Spectral-Domain and Swept-Source Optical Coherence Tomography Angiographic Imaging of Choroidal Neovascularization

Andrew R. Miller,[1] Luiz Roisman,[1,2] Qinqin Zhang,[3] Fang Zheng,[1] Joao Rafael de Oliveira Dias,[1] Zohar Yehoshua,[1] Karen B. Schaal,[1] William Feuer,[1] Giovanni Gregori,[1] Zhongdi Chu,[3] Chieh-Li Chen,[3] Sophie Kubach,[4] Lin An,[4] Paul F. Stetson,[4] Mary K. Durbin,[4] Ruikang K. Wang,[3] and Philip J. Rosenfeld[1]

[1]Department of Ophthalmology, Bascom Palmer Eye Institute, University of Miami Miller School of Medicine, Miami, Florida, United States
[2]Department of Ophthalmology, Federal University of São Paulo, São Paulo, Brazil
[3]Department of Bioengineering, University of Washington, Seattle, Washington, United States
[4]Advanced Development, Carl Zeiss Meditec, Inc., Dublin, California, United States

PURPOSE. The purpose of this study was to compare imaging of choroidal neovascularization (CNV) using swept-source (SS) and spectral-domain (SD) optical coherence tomography angiography (OCTA).

METHODS. Optical coherence tomography angiography was performed using a 100-kHz SS-OCT instrument and a 68-kHz SD-OCTA instrument (Carl Zeiss Meditec, Inc.). Both 3×3- and 6×6-mm^2 scans were obtained on both instruments. The 3×3-mm^2 SS-OCTA scans consisted of 300 A-scans per B-scan at 300 B-scan positions, and the SD-OCTA scans consisted of 245 A-scans at 245 B-scan positions. The 6×6-mm^2 SS-OCTA scans consisted of 420 A-scans per B-scan at 420 B-scan positions, and the SD-OCTA scans consisted of 350 A-scans and 350 B-scan positions. B-scans were repeated four times at each position in the 3×3-mm^2 scans and twice in the 6×6-mm^2 scans. Choroidal neovascularization was excluded if not fully contained within the 3×3-mm^2 scans. The same algorithm was used to detect CNV on both instruments. Two graders outlined the CNV, and the lesion areas were compared between instruments.

RESULTS. Twenty-seven consecutive eyes from 23 patients were analyzed. For the 3×3-mm^2 scans, the mean lesion areas for the SS-OCTA and SD-OCTA instruments were 1.17 and 1.01 mm^2, respectively ($P = 0.047$). For the 6×6-mm^2 scans, the mean lesion areas for the SS-OCTA and SD-OCTA instruments were 1.24 and 0.74 mm^2 ($P = 0.003$).

CONCLUSIONS. The areas of CNV tended to be larger when imaged with SS-OCTA than with SD-OCTA, and this difference was greater for the 6×6-mm^2 scans.

Keywords: optical coherence tomography angiography, OCTA, swept-source OCTA, spectral-domain OCTA, neovascular AMD, choroidal neovascularization

Optical coherence tomography (OCT) has become a valuable imaging strategy for diagnosing and following patients with neovascular AMD (nvAMD).[1] Until recently, OCT imaging could only identify some of the structural changes in the macula associated with neovascularization, including macular fluid and hyperreflective material in the retina, under the retina, and under the RPE, but could not identify the underlying vascular changes. With the development of OCT angiography (OCTA), it is now possible to directly image the neovascularization in the retina (type 3),[2,3] under the retina and above the RPE (type 2),[4,5] and under the RPE (type 1).[6,7] To detect this vascular flow information, the OCTA algorithms generate images based on the motion signal between repeated OCT B-scans at the same position. This signal, which reflects subtle differences between B-scans at the same position, is mostly due to the movement of erythrocytes within blood vessels.[8] Although different OCTA instruments use different hardware configurations and different motion contrasting algorithms, the basic premise for the detection of blood flow remains the same for all the different OCTA imaging strategies.

Both spectral-domain (SD) and swept-source OCTA instruments have been used to detect choroidal neovascularization (CNV).[9,10] Both instruments use Fourier domain detection techniques, but the SD-OCT instruments use a broadband near-infrared superluminescent diode as a light source, currently with a center wavelength of approximately 840 nm, with a spectrometer as the detector, whereas the SS-OCT instruments use a tunable swept laser, currently with a center wavelength of approximately 1050 nm, with a single photodiode detector.[11] One of the advantages of SS-OCTA imaging over SD-OCTA is the faster scanning speed, which allows for denser scan patterns and larger scan areas compared with SD-OCT scans for a given

acquisition time. Additional advantages of the current SS-OCT technology are its use of a longer wavelength and its reduced sensitivity roll-off, resulting in enhanced light penetration through the RPE, as well as better detection of signals from the deeper layers. The longer wavelength is also safer for the eye so a higher laser power can be used. The higher power combined with the reduced sensitivity roll-off improves the likelihood of detecting the inherently weaker signals from deeper layers. Overall, these advantages should help the SS-OCT system overcome the barrier of the RPE, resulting in better detection of type 1 CNV compared with SD-OCTA imaging.[9] Although SD-OCTA imaging has been shown to detect some CNV in nvAMD,[2–7,9,12] there appear to be limitations in the ability of SD-OCTA to detect neovascularization under the RPE, as reported in cases when a CNV is known to be present from dye-based angiographic imaging and structural alterations, but SD-OCTA did not detect the neovascular lesion.[9,12,13] A recent report compared the ability of both SD-OCTA and SS-OCTA to detect CNV, concluding that SS-OCTA imaging appeared to be better than SD-OCTA in detecting CNV. Possible explanations for why SS-OCTA was better than SD-OCTA for the detection of CNV not only include the longer wavelength of the swept source laser with its better sensitivity roll-off and higher laser power, but also its higher scanning speeds, which permitted higher A-scan and B-scan densities and a greater number of B-scan repeats at each position for a given acquisition time and scan area. Other important differences between the two imaging techniques included different image processing algorithms and the use of different segmentation strategies to determine the full extent of the neovascular lesions.[9] Although we can't control for the laser wavelength, scanning speeds, sensitivity roll-off, or scanning densities when comparing the two imaging strategies, we can control for the algorithms used to process the scans and the segmentation strategy used to visualize the CNV.

To compare the detection of CNV in nvAMD using both SD-OCTA and SS-OCTA imaging, we performed a study with a commercially available SD-OCTA instrument and a prototype SS-OCTA instrument. Carl Zeiss Meditec, Inc. (Dublin, CA, USA) manufactured both instruments. The output data from both instruments were analyzed using the same segmentation slabs, the same motion contrasting algorithm known as optical microangiography (OMAG^C), and the same retinal vascular projection artifact removal algorithm.

PATIENTS AND METHODS

Patients were enrolled at the Bascom Palmer Eye Institute in a prospective OCT imaging study. The Institutional Review Board of the University of Miami Miller School of Medicine approved the study, and an informed consent to participate in the prospective OCT study was obtained from all patients. The study was performed in accordance with the tenets of the Declaration of Helsinki and compliant with the Health Insurance Portability and Accountability Act of 1996.

Patients with the diagnosis of CNV secondary to AMD previously identified by conventional SD-OCT structural imaging or dye-based conventional angiography were scanned on both the SD-OCTA and SS-OCTA instruments by the same technician during the same imaging session. Spectral-domain OCTA imaging was performed using of a Cirrus AngioPlex device provided by Carl Zeiss Meditec, Inc. This instrument had a center wavelength of 840 nm, a bandwidth of 90 nm, an A-scan depth of 2.0 mm in tissue (1024 pixels), a full width at half maximum (FWHM) axial resolution of ~5 μm in tissue, a lateral resolution at the retinal surface estimated at ~15 μm, and a scanning rate of 68,000 A-scans per second. All scans

were centered on the fovea, and FastTrac motion correction software (Carl Zeiss Meditec, Inc.) was used while the images were acquired. For the 3 × 3-mm² SD-OCTA scans, each B-scan contained 245 A-scans per B-scan along the fast x-axis, and each B-scan was repeated four times at each position. There were 245 B-scan positions along the slow y-axis. As a result, we had a homogenous sampling grid with a separation of 12.2 μm. For the 6 × 6-mm² SD-OCTA scans, each B-scan contained 350 A-scans per B-scan along the fast x-axis, and each B-scan was repeated two times at each position. There were 350 B-scan positions along the slow y-axis. As a result, we had a homogenous sampling grid with a separation of 17.1 μm.

Swept-source OCTA was performed using a prototype provided by Carl Zeiss Meditec, Inc. This instrument is characterized by a central wavelength of 1050 nm, a bandwidth of 100 nm, an A-scan depth of 3.0 mm in tissue (1536 pixels), a FWHM axial resolution of ~5 μm in tissue, a lateral resolution at the retinal surface estimated at ~14 μm, and a scanning rate of 100,000 A-scans per second. FastTrac motion correction software was used while the images were acquired. Scan protocols were similar to those described for the SD-OCTA system but with an increased density of A-scans per B-scan and B-scan positions. The 3 × 3-mm² SS-OCTA scans used 300 A-scans per B-scan repeated four times at each of the 300 B-scan positions. As a result, we had a homogenous sampling grid with a separation of 10 μm. The 6 × 6-mm² SS-OCTA scans used 420 A-scans per B-scan repeated twice at each of the 420 B-scan locations. As a result, we had a homogenous sampling grid with a separation of 14.3 μm.

Visualization of the retinal and choroidal vasculature from the volumetric datasets was achieved using a method known as optical microangiography, based on the complex OCT signal (OMAG^C).[8] The OMAG^C algorithm incorporates variations in both the intensity and phase information between sequential B-scans at the same position to generate the flow information. En face flow images were obtained using previously described strategies for segmentation and removal of the decorrelation projection artifacts.[10,14–16] The same segmentation and image processing strategies were applied to both the SD-OCTA and SS-OCTA datasets. The segmentation boundaries for the slab used in this study extended from the outer boundary of the outer plexiform layer (OPL) to 8 μm beneath Bruch's membrane. This slab, referred to as the outer retina to choriocapillaris (ORCC) slab, should contain both type 1 and type 2 CNV.[10,17] Removal of the retinal projection artifacts from overlying retinal vasculature onto the ORCC slab was performed as previously described.[10,15–17] The en face ORCC slab flow image following projection artifact removal was displayed as a grayscale image for grading each neovascular lesion's area.

To be included in this study, the CNV had to be entirely contained within the 3 × 3-mm² en face ORCC slab flow image obtained from both the SS-OCTA and SD-OCTA datasets. In addition, images had to have a signal strength of at least six without the presence of excessive motion artifacts. The images were assembled randomly into two datasets of 3 × 3-mm² scans and 6 × 6-mm² scans. Two graders (JROD and ZY) outlined each neovascular lesion using Adobe Photoshop Creative Cloud (Release 2015.1.2; Adobe Systems, Inc., San Jose, CA, USA) and a Wacom pen tablet (Wacom Technology Corporation, Portland, OR, USA). Graders outlined the images in two sessions. They were masked as to which instrument was used to acquire the image. If the graders felt that no neovascular lesion could be clearly demarcated, then no image was outlined. After grading the images separately, the graders reached a consensus outline for each image, and if any lingering disagreements persisted, the senior grader (PJR) adjudicated the case. None of the graders reviewed the images

prior to grading. Training of graders was performed using OCTA images from both instruments that were not included in the final grading. Pixel counts from the outlined area were measured using Adobe Photoshop, and the pixel counts were converted into area measurements.

Lesion areas obtained using the SD-OCTA and SS-OCTA datasets, as well as Bland-Altman analyses for the differences in area measurements, are reported. Statistical analysis was performed with IBM SPSS Statistics for Windows, Version 22.0 (IBM Corporation, Armonk, NY, USA).

RESULTS

Comparing Measurements of CNV Between Two Devices

One hundred fifteen eyes from 90 patients with nvAMD were imaged as described above. Thirty-five eyes were excluded because the CNV was not fully contained within the 3×3-mm^2 scan area. An additional 53 eyes were excluded because of signal quality problems with at least one of the four scans, which included scans with signal strength below six or excessive motion artifacts.

Twenty-seven eyes from 23 patients with neovascular AMD imaged from October 2015 to April 2016 were identified as candidates for this study. Thirteen (56%) of the 23 patients were men. Mean patient age was 77.4 years old and ranged from 51 to 88 years old. At the time of imaging, 25 of 27 eyes had received prior intravitreal therapy with VEGF inhibitors, 1 eye received an injection on the day of imaging due to new onset exudation, and 1 eye had CNV without exudation and was being observed as previously described.[10]

Of the 108 images outlined by the graders, only one image needed adjudication by the senior grader. Neovascular lesions were identified in all 3×3-mm^2 images from both the SD-OCTA and SS-OCTA instruments. However, in four 6×6-mm^2 images, one SS-OCTA scan and three SD-OCTA scans, the graders could not outline a neovascular lesion, resulting in area measurements equal to 0 mm^2.

Overall, the area measurements obtained from the SS-OCTA instrument were significantly larger than the area measurements from the SD-OCTA instrument for the 3×3-mm^2 and 6×6-mm^2 scans, and this difference was more pronounced for the 6×6-mm^2 scans. Mean area measurements for the 3×3-mm^2 scans from the SS-OCTA and SD-OCTA instruments were 1.17 and 1.01 mm^2, respectively ($P = 0.047$). Mean area measurements for the 6×6-mm^2 scans from the SS-OCTA and SD-OCTA instruments were 1.24 and 0.74 mm^2 ($P = 0.003$). Figure 1 shows an example of a neovascular lesion that had similar area measurements with both the SD-OCTA and SS-OCTA instruments. Figure 2 shows an example of a neovascular lesion that had a larger area measurement with the SS-OCTA instrument compared with the SD-OCTA instrument. Figure 3 is an example of a nonexudative neovascular lesion in which the quiescent lesion could be imaged using the 3×3-mm^2 scan from both instruments, with a larger measurement arising from the SS-OCTA scan, but this neovascular lesion could not be adequately imaged using the SD-OCTA instrument's 6×6-mm^2 scan. As seen in the examples, the major differences in the area measurements occurred at the margins of the lesions. Measurements from the SD-OCTA and SS-OCTA scans are compared in the scatter plots shown in Figure 4 and the Bland-Altman analyses shown in Figure 5. Overall, the hand-drawn area measurements were larger for the SS-OCTA scans, and this was particularly obvious for the 6×6-mm^2 scans with a number of eyes showing larger area measurements on SS-OCTA imaging compared with the 3×3-mm^2 scans (Figs. 4, 5).
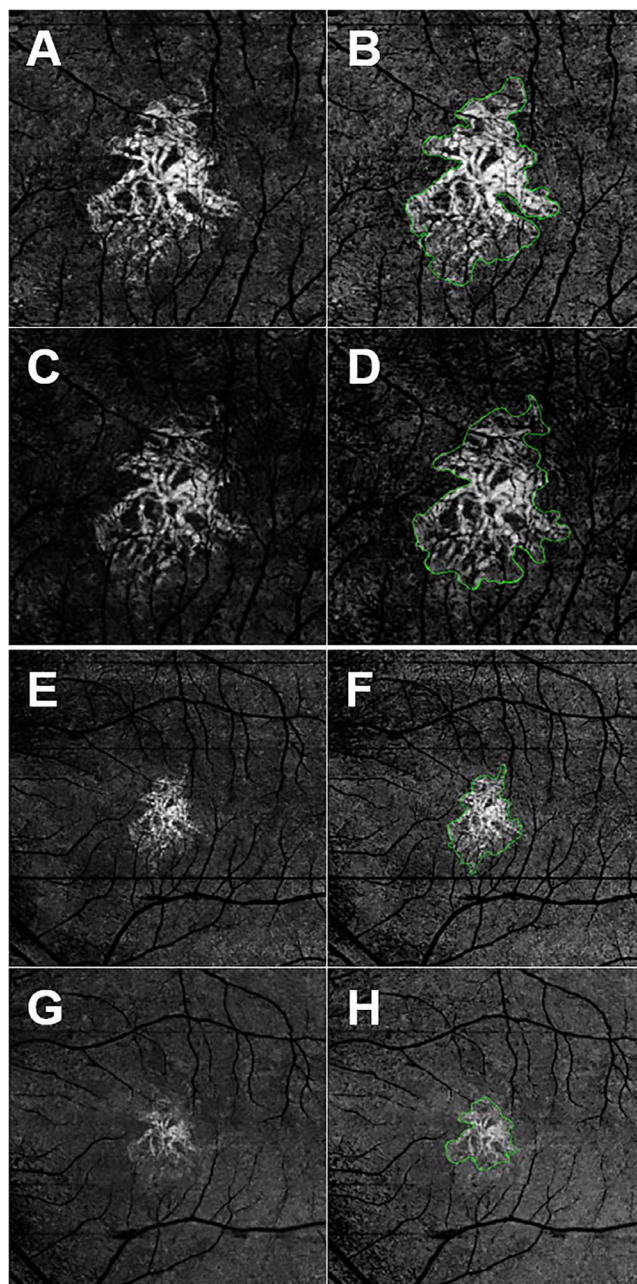
FIGURE 1. En face SS- and SD-OCTA images from the left eye of a 70-year-old woman with CNV secondary to AMD. All images were processed from the corresponding volumetric datasets using the same algorithms that were applied to a slab that extended from the outer retina to the choriocapillaris and included the removal of the projection artifacts from the retinal vasculature. (**A**) Swept-source OCTA 3×3-mm^2 scan. (**B**) Swept-source OCTA 3×3-mm^2 scan with an outline of the CNV and an area of 1.51 mm^2. (**C**) Spectral-domain OCTA 3×3-mm^2 scan. (**D**) Spectral-domain OCTA 3×3-mm^2 scan with an outline of the CNV and an area of 1.51 mm^2. (**E**) Swept-source OCTA 6×6-mm^2 scan. (**F**) Swept-source OCTA 6×6-mm^2 scan with an outline of the CNV and an area of 1.52 mm^2. (**G**) Spectral-domain OCTA 6×6-mm^2 scan. (**H**) Spectral-domain OCTA 6×6-mm^2 scan with an outline of the CNV and an area of 1.13 mm^2. In this example, the area measurements were similar for the 3×3-mm^2 scans, but SS-OCTA imaging showed a larger lesion for the 6×6-mm^2 scans.
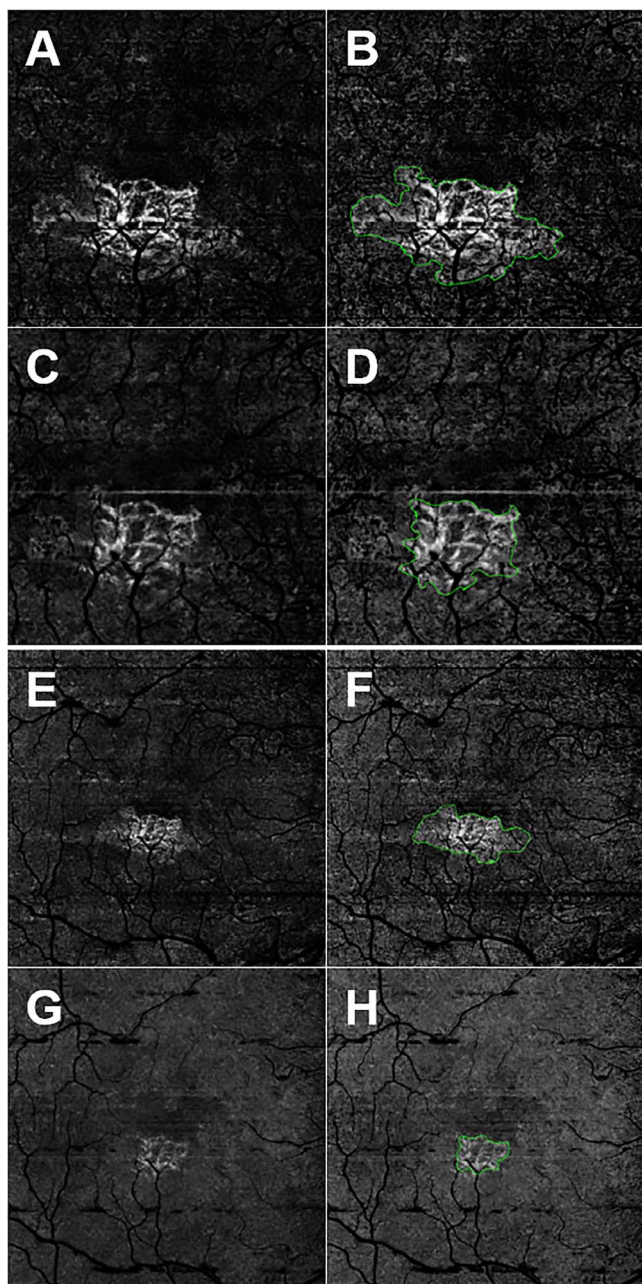
FIGURE 2. En face SS- and SD-OCTA images from the left eye of an 87-year-old woman with CNV secondary to AMD. All images were processed from the corresponding volumetric datasets using the same algorithms that were applied to a slab that extended from the outer retina to the choriocapillaris and included the removal of the projection artifacts from the retinal vasculature. (A) Swept-source OCTA 3×3-mm^2 scan. (B) Swept-source OCTA 3×3-mm^2 scan with an outline of the CNV and an area of 1.25 mm^2. (C) Spectral-domain OCTA 3×3-mm^2 scan. (D) Spectral-domain OCTA 3×3-mm^2 scan with an outline of the CNV and an area of 0.722 mm^2. (E) Swept-source OCTA 6×6-mm^2 scan. (F) Swept-source OCTA 6×6-mm^2 scan with an outline of the CNV and an area of 1.40 mm^2. (G) Spectral-domain OCTA 6×6-mm^2 scan. (H) Spectral-domain OCTA 6×6-mm^2 scan with an outline of the CNV and an area of 0.535 mm^2. In this example, SS-OCTA imaging yielded the larger area measurements for both the 3×3- and 6×6-mm^2 scans compared with SD-OCTA imaging.
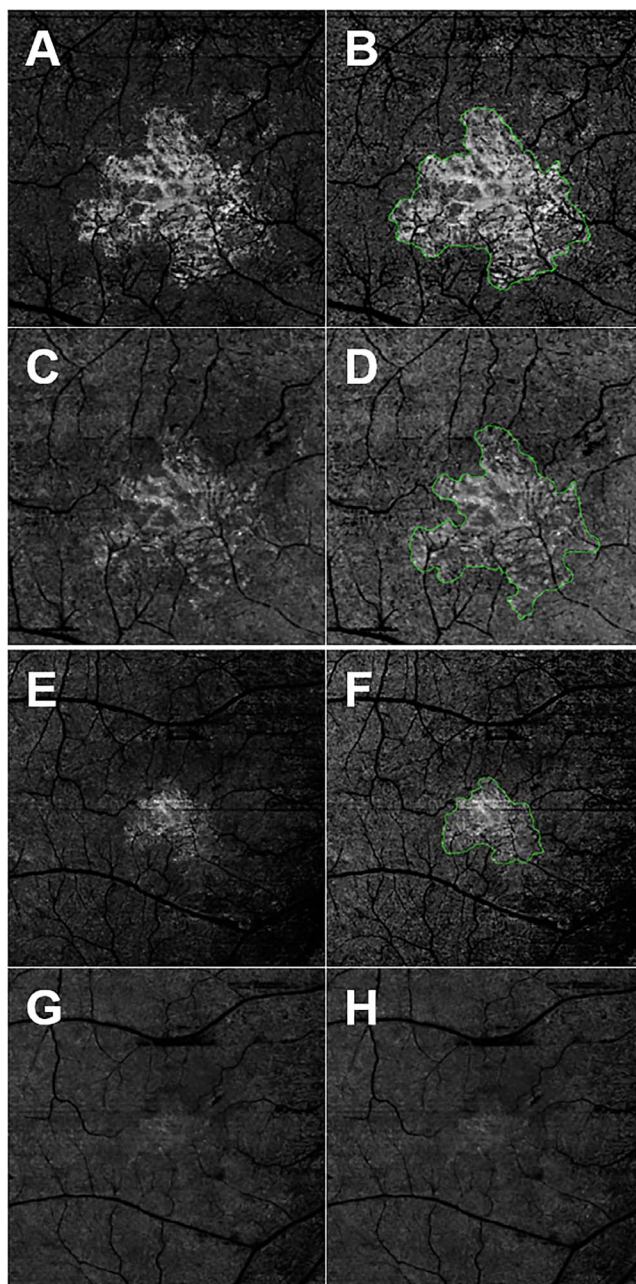
FIGURE 3. En face SS- and SD-OCTA images from the left eye of a 79-year-old man with CNV secondary to AMD. All images were processed from the corresponding volumetric datasets using the same algorithms that were applied to a slab that extended from the outer retina to the choriocapillaris and included the removal of the projection artifacts from the retinal vasculature. (A) Swept-source OCTA 3×3-mm^2 scan. (B) Swept-source OCTA 3×3-mm^2 scan with an outline of the CNV and an area of 1.75 mm^2. (C) Spectral-domain OCTA 3×3-mm^2 scan. (D) Spectral-domain OCTA 3×3-mm^2 scan with an outline of the CNV and an area of 1.60 mm^2. (E) Swept-source OCTA 6×6-mm^2 scan. (F) Swept-source OCTA 6×6-mm^2 scan with an outline of the CNV and an area of 1.95 mm^2. (G) Spectral-domain OCTA 6×6-mm^2 scan. (H) Spectral-domain OCTA 6×6-mm^2 scan without any outline of the CNV due to the consensus between graders that the lesion borders for the CNV were not clearly demarcated.
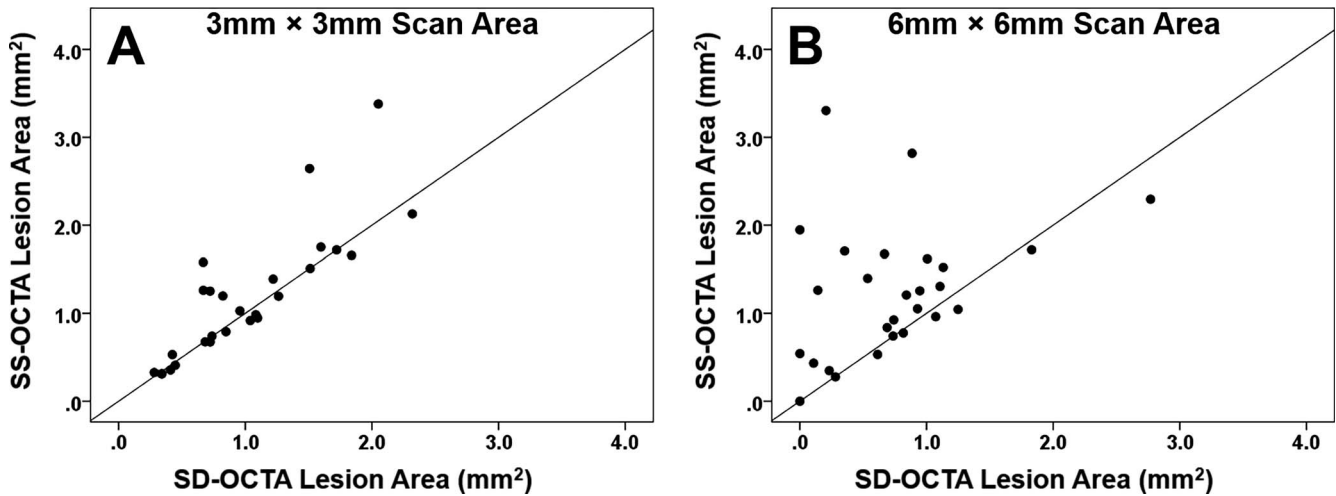
FIGURE 4. Scatter plots comparing area measurements of CNV obtained using 3×3- and 6×6-mm² SS- and SD-OCTA scans. (**A**) Comparison between 3×3-mm² CNV area measurements from the SS-OCTA and SD-OCTA instruments. Slightly larger CNV areas were measured using the SS-OCTA instrument ($P = 0.047$), but the correlation coefficient was good at $r = 0.84$ ($P < 0.001$). (**B**) Comparison between 6×6-mm² CNV area measurements from the SS-OCTA and SD-OCTA instruments. Larger CNV areas were measured using the SS-OCTA instrument ($P = 0.003$), and the correlation coefficient was modest at $r = 0.33$ ($P = 0.093$).

Moreover, the 3×3-mm² scans showed a much better correlation between the area measurements from the two instruments ($r = 0.84$, $P < 0.001$) compared with the 6×6-mm² scan measurements ($r = 0.33$, $P = 0.093$). In addition, larger differences in area measurements were associated with larger lesions (Fig. 5).

Comparing Contrast-to-Noise Between Two Devices

Image quality can play an important role when the ORCC angiograms are compared. We hypothesized that the better light penetration, sensitivity, and scan density of the SS-OCTA images should result in better image quality for the OCTA ORCC angiograms, which should lead to more reliable measurements of CNV. To test this hypothesis, we compared the image quality of the ORCC angiograms delivered by SD-OCTA and SS-OCTA using the contrast-to-noise ratio (CNR).

Contrast-to-noise ratio is similar to the signal-to-noise ratio, but subtracts off a term corresponding to the noise background before taking the ratio. This is important when there is a significant bias in an image, such as nonzero mean noise background, which is true for OCT images. In the evaluation, we defined CNR as follows[18]:

$$\text{CNR} = \frac{|\mu_s - \mu_n|}{\sigma}$$

where μ_s is the signal mean; μ_n is the mean of the background noise; and σ is the standard deviation of the background noise. After the calculation of CNRs for all the ORCC angiograms obtained from the enrolled eyes, we performed a subgroup analysis between the devices and between the fields of view. We found that the mean values of CNR for the 3×3-mm² scans are 2.42 and 2.08 for the SS-OCTA– and SD-OCTA–derived ORCC angiograms, respectively, and for the 6×6-mm² scans, the mean values of the CNR are 1.96 and 1.12 for the SS-OCTA–
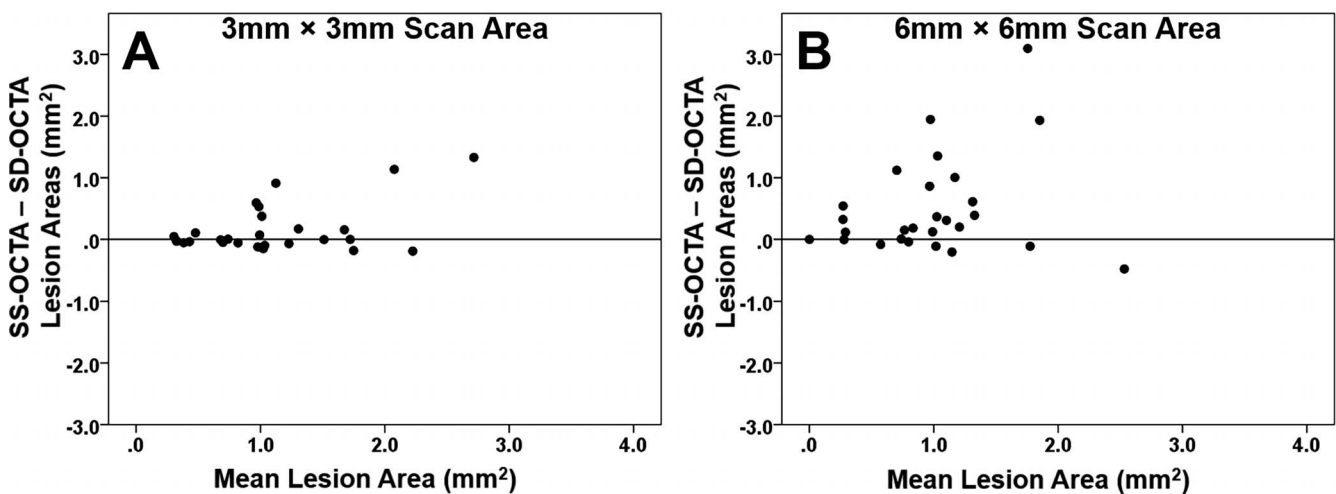

FIGURE 5. Bland-Altman plots showing the difference in area measurements of CNV obtained using SS- and SD-OCTA scans with both the 3×3- and 6×6-mm² scan patterns. (**A**) Difference in area measurements between SS-OCTA and SD-OCTA imaging using the 3×3-mm² scan and the relationship with mean lesion area. (**B**) Difference in area measurements between SS-OCTA and SD-OCTA imaging using the 6×6-mm² scan and the relationship with mean lesion area.

TABLE. Comparison Between CNR Values of SS-OCTA– and SD-OCTA–Derived ORCC Angiograms

	3 × 3-mm² Scans		6 × 6-mm² Scans	
CNR	SD-OCTA	SS-OCTA	SD-OCTA	SS-OCTA
Mean (minimum, maximum)	2.08 (0.94, 4.93)	2.42 (0.91, 4.89)	1.12 (0.35, 2.53)	1.96 (0.87, 3.13)
Standard deviation	0.90	0.96	0.56	0.58
P value		0.008		<0.001

and SD-OCTA–derived ORCC angiograms, respectively. The comparison is summarized in the Table. Significantly higher CNR values were found in both the fields of view for SS-OCTA images, indicating that SS-OCTA has the capability to deliver ORCC angiograms with better image quality compared with SD-OCTA.

Discussion

Both SS-OCTA and SD-OCTA imaging can detect CNV, but SS-OCTA detects on average a larger area for the CNV than detected using SD-OCTA imaging. Whether the actual CNV is even larger than the area detected by SS-OCTA remains to be determined, but in our previous report describing indocyanine green angiography (ICGA) imaging of nonexudative CNV in AMD, we found that the SS-OCTA images were comparable to the size and configuration of the plaques identified on ICGA imaging.[10] The results presented in this current report indicate that en face SS-OCTA imaging provided a more accurate representation of the CNV compared with SD-OCTA imaging, in particular the SS-OCTA measurements are more consistent across the different scan sizes. The area measurements on SS-OCTA imaging were larger for both the 3 × 3-mm² scans ($P = 0.047$) and the 6 × 6-mm² scans ($P = 0.003$). The difference in lesion areas was much larger for the 6 × 6-mm² scans than the 3 × 3-mm² scans. The higher variability in the measurements obtained with the 6 × 6-mm² scans compared with the 3 × 3-mm² scans, is consistent with the CNR reported above. We found that the angiograms from the 3 × 3-mm² scans provided a higher CNR compared with that of 6 × 6-mm² scans. The lower CNR values for the 6 × 6-mm² scans might be attributed to two reasons: the pixel spacing was larger than in the 3 × 3-mm² scans (14.3 vs. 10 μm for SS-OCTA and 17.1 vs. 12.2 μm for SD-OCTA) and the repetition numbers of B-scans at one spatial location was lower than in the 3 × 3-mm² scans (2 vs. 4). The lower CNR values for 6 × 6-mm² scans is likely responsible for the observed limitations in the reproducibility of CNV measurements. It is important to note that the CNR values of 1.96 for the SS-OCTA 6 × 6-mm² scan is close to that of 2.08 for SD-OCTA 3 × 3-mm² scan, despite using only two repeated B-scans to obtain the OCT angiographic signals (instead of four). Although we were unable to control for the scanning densities used in both instruments, our analysis of the CNR values would suggest that the higher scanning densities used in SS-OCTA imaging contributed to its superior detection of CNV compared with SD-OCTA imaging. Moreover, the superiority of SS-OCTA detection of CNV using a 6 × 6-mm² scan pattern has real-world clinical relevance given the fact that CNV routinely extends outside the central 3 × 3-mm² scan pattern, and identifying the full extent of the CNV would be important for the detection and follow-up of these lesions.

Previously, Novais et al.[9] compared the visualization of CNV in nvAMD using both SD-OCTA and SS-OCTA; however, they used different segmentation strategies when analyzing the images from each instrument. Because we know that segmentation boundaries greatly influence the ability to visualize the entire CNV, we felt it was necessary to repeat their study using the same segmentation strategy. To achieve these objectives, the SD-OCTA and SS-OCTA datasets were downloaded directly from the instruments and processed using custom application software.[8,10,14–16] Our study used the same OMAG algorithm to generate the decorrelation signals, the same algorithm to generate the segmentation boundaries, and the same algorithm for the removal of the retinal vessel projection artifacts.

Limitations of our study include a small sample size, the use of segmentation and image processing strategies that were not commercially available at this time, and the need to exclude a large number of eyes, either because the CNV was not entirely contained in a 3 × 3-mm² scan or because of problems with scan quality. The requirement for all the scans to be of the highest image quality and the exclusion of poor quality scans was intended to allow for the best possible quantitative comparison between instruments, but many of the images would have sufficed in the routine clinical care of patients when qualitative assessment of CNV was all that was needed. Overall, there were no differences between instruments with respect to signal strength and motion artifacts. In addition, we only examined lesions fully contained within the 3 × 3-mm² scan to obtain a sample where the two scan sizes could be fully compared and a possible difference in performance based on the different scanning densities could be assessed. One reason for decreased signal strength appeared to be the presence of a cataract; however, a more detailed study is needed to address the imaging of CNV through cataracts using the different devices.

Given the findings previously reported by Novais et al.,[9] it should come as no surprise that SS-OCTA imaging was better at detecting CNV than SD-OCTA imaging. This ability to detect the presence and size of CNV through an intact RPE should prove particularly useful in eyes with nonexudative AMD in which CNV is present but macular fluid is absent.[10,19,20] More significantly, there is speculation that the portion of the neovascular lesion that might need to be visualized to predict future growth and exudation is the region at the borders of the lesion, and it is this border region that SS-OCTA is better at visualizing than SD-OCTA imaging. In addition, when using OCTA to follow eyes with exudative CNV to determine when retreatment might be needed, the ability to detect the entire lesion and changes at the borders of the lesion could very well influence the retreatment decision.

Previously, De Carlo et al.[12] reported a specificity of 91% but a sensitivity of only 50% for detecting CNV using SD-OCTA. Most likely, SS-OCTA imaging would have a significantly better sensitivity. The improved detection of CNV by SS-OCTA also raises an interesting question about the current and future gold standard for imaging CNV. Given the shorter time of acquisition, lower cost of acquisition, greater convenience, greater comfort, and greater safety of imaging with OCTA compared with dye-based angiography, it is just a matter of time before SS-OCTA becomes the gold standard for imaging CNV. The greatest limitations for the widespread use of this imaging technique are the high cost of purchasing the instruments and the availability of the instruments, but these

limitations should be resolved in the very near future. Moreover, with increasing scanning rates, which will result in larger scan areas with higher sampling densities, and with better tracking software on the horizon, we anticipate that the upper limit for detection of CNV has not yet been achieved.

In summary, when using the instruments and algorithms described in this report, we found that SS-OCTA imaging was able to detect CNV better than SD-OCTA imaging. Although the algorithms used in this study are not yet commercially available, they are currently being developed for commercial application and should be available in the very near future.

References

1. Rosenfeld PJ. Optical coherence tomography and the development of antiangiogenic therapies in neovascular age-related macular degeneration. *Invest Ophthalmol Vis Sci*. 2016;57: 14–26.

2. Kuehlewein L, Dansingani KK, de Carlo TE, et al. Optical coherence tomography angiography of type 3 neovascularization secondary to age-related macular degeneration. *Retina*. 2015;35:2229–2235.

3. Querques G, Miere A, Souied EH. Optical coherence tomography angiography features of type 3 neovascularization in age-related macular degeneration. *Dev Ophthalmol*. 2016;56:57–61.

4. Kuehlewein L, Sadda SR, Sarraf D. OCT angiography and sequential quantitative analysis of type 2 neovascularization after ranibizumab therapy. *Eye*. 2015;29:932–935.

5. Souied EH, El Ameen A, Semoun O, Miere A, Querques G, Cohen SY. Optical coherence tomography angiography of type 2 neovascularization in age-related macular degeneration. *Dev Ophthalmol*. 2016;56:52–56.

6. Kuehlewein L, Bansal M, Lenis TL, et al. Optical coherence tomography angiography of type 1 neovascularization in age-related macular degeneration. *Am J Ophthalmol*. 2015;160: 739–748.

7. Iafe NA, Phasukkijwatana N, Sarraf D. Optical coherence tomography angiography of type 1 neovascularization in age-related macular degeneration. *Dev Ophthalmol*. 2016;56:45–51.

8. Huang Y, Zhang Q, Thorell MR, et al. Swept-source OCT angiography of the retinal vasculature using intensity differentiation-based optical microangiography algorithms. *Ophthal Surg Lasers Imaging Retina*. 2014;45:382–389.

9. Novais EA, Adhi M, Moult EM, et al. Choroidal neovascularization analyzed on ultrahigh-speed swept-source optical coherence tomography angiography compared to spectral-domain optical coherence tomography angiography. *Am J Ophthalmol*. 2016;164:80–88.

10. Roisman L, Zhang Q, Wang RK, et al. Optical coherence tomography angiography of asymptomatic neovascularization in intermediate age-related macular degeneration. *Ophthalmology*. 2016;123:1309–1319.

11. Potsaid B, Baumann B, Huang D, et al. Ultrahigh speed 1050nm swept source/Fourier domain OCT retinal and anterior segment imaging at 100,000 to 400,000 axial scans per second. *Optics Express*. 2010;18:20029–20048.

12. de Carlo TE, Bonini Filho MA, Chin AT, et al. Spectral-domain optical coherence tomography angiography of choroidal neovascularization. *Ophthalmology*. 2015;122:1228–1238.

13. Inoue M, Jung JJ, Balaratnasingam C, et al. A comparison between optical coherence tomography angiography and fluorescein angiography for the imaging of type 1 neovascularization. *Invest Ophthalmol Vis Sci*. 2016;57:314–323.

14. Yin X, Chao JR, Wang RK. User-guided segmentation for volumetric retinal optical coherence tomography images. *J Biomed Optics*. 2014;19:086020.

15. Zhang A, Zhang Q, Wang RK. Minimizing projection artifacts for accurate presentation of choroidal neovascularization in OCT micro-angiography. *Biomed Optics Express*. 2015;6: 4130–4143.

16. Zhang Q, Zhang A, Lee CS, et al. Projection artifact removal improves visualization and quantitation of macular neovascularization imaged by optical coherence tomography angiography. *Ophthalmology Retina*. 2017;1:124–136.

17. Zhang Q, Wang RK, Chen CL, et al. Swept source optical coherence tomography angiography of neovascular macular telangiectasia type 2. *Retina*. 2015;35:2285–2299.

18. Welvaert M, Rosseel Y. On the definition of signal-to-noise ratio and contrast-to-noise ratio for FMRI data. *PLoS One*. 2013;8:e77089.

19. Palejwala NV, Jia Y, Gao SS, et al. Detection of nonexudative choroidal neovascularization in age-related macular degeneration with optical coherence tomography angiography. *Retina*. 2015;35:2204–2211.

20. Nehemy MB, Brocchi DN, Veloso CE. Optical coherence tomography angiography imaging of quiescent choroidal neovascularization in age-related macular degeneration. *Ophthal Surg Lasers Imaging Retina*. 2015;46:1056–1057.